

# Synthesis and Characterization of $\text{Al}(\text{OH})_3$ , $\text{Al}_2\text{O}_3$ Nanoparticles and Polymeric Nanocomposites

Mojgan Goudarzi<sup>1</sup> · Davood Ghanbari<sup>2</sup> ·  
Masoud Salavati-Niasari<sup>1</sup> · Amin Ahmadi<sup>3</sup>

Received: 17 April 2015 / Published online: 19 June 2015  
© Springer Science+Business Media New York 2015

**Abstract** Applying of the most toxic halogenated and aromatic flame retardants is limited with respect to the environmental requirements. Nontoxic  $\text{Al}(\text{OH})_3$  nanoparticles were synthesized via a simple surfactant-free precipitation reaction at room temperature. The effect of various precipitation-agents on the morphology of the products was investigated.  $\text{Al}(\text{OH})_3$  nanoparticles were added to the polysulfone and poly styrene (PS) matrices. Electron microscope images show excellent dispersion of aluminium hydroxide in PS matrix. Nanoparticles appropriately enhanced both thermal stability and flame retardant property of the polymeric matrices. The enhancement of flame retardancy is due to endothermic decomposition of  $\text{Al}(\text{OH})_3$  that absorbs heat and simultaneously releases of water (makes combustible gases diluted and cold). Dispersed nanoparticles play the role of a barrier layer against flame, oxygen and polymer volatilization.  $\text{Al}(\text{OH})_3$  was converted to  $\text{Al}_2\text{O}_3$  and its photo-catalyst property in degradation three different organic dyes as pollutants was investigated.

**Keywords** Nanoparticles · Aluminium hydroxide · Nanocomposite · Thermal stability

---

✉ Masoud Salavati-Niasari  
Salavati@kashanu.ac.ir

<sup>1</sup> Institute of Nano Science and Nano Technology, University of Kashan,  
P.O. Box 87317-51167, Kashan, Islamic Republic of Iran

<sup>2</sup> Young Researchers and Elite Club, Arak Branch, Islamic Azad University, Arrack,  
Islamic Republic of Iran

<sup>3</sup> Department of Mechanic, Kashan Branch, Islamic Azad University, Kashan,  
Islamic Republic of Iran

## Introduction

One of the most commonly used mineral flame retardants is aluminum hydroxide. As the temperature increases aluminum hydroxide shows endothermic decomposition (about 220 °C with an endothermic reaction of 1.17 kJ/g) and absorbs energy. It also releases nonflammable water which dilutes combustible gases. Aluminum oxide provides heat insulation by reflecting heat when it accumulates on the surface. It's widely used because of its low cost and non-toxicity and easy to incorporate into various thermo-sets polymers [1–5]. One of the main disadvantages of non-nanostructure  $\text{Al}(\text{OH})_3$  is that for pass flame retardancy tests, 30–65 wt% of aluminum hydroxide is required. Increasing the loading of inorganic metal hydroxides will result in a significant decrease in physical properties. So synthesis of  $\text{Al}(\text{OH})_3$  nanostructures has attracted much attention in recent years owing to their unique properties and wide applications in plastics, rubbers, papers, glasses and medicines, and so forth [6–11]. In addition aluminum hydroxide is an important precursor for synthesis of alumina and alumina-derived ceramics. Alumina has many desired properties such as high surface area, good mechanical and especially thermal and chemical stability etc. So alumina (specially gamma phase) has various industrial applications, and can be widely used as absorbent, catalyst, heat transfer and catalyst support [12–16]. Due to the significant advantages of gamma phase, its synthesis is highly regarded. The high purity nanocrystalline alumina powders were synthesized as yet by variety methods such as precipitation, hot-air spray pyrolysis, sol-gel and hydrothermal [17–22].

Nanostructures have been intensively studied in a wide range of application because the properties of nanocrystals depend not only on their composition but also on their shape, size, structure, phase, and size distribution. The reactivity and selectivity of nanoparticles can be adjusted by controlling the morphology because the exposed surfaces of the particles have distinct crystallographic planes depending on the shape. Polymeric nanocomposites have gained much attention because adding a small amount of nanostructure to a polymeric matrix can lead to improvement properties of the matrix. The principal profits of these compounds over many metallic alloys are corrosion resistance, low density and thermal insulation. However the main disadvantage of polymeric compounds is high flammability. Using of the most traditional and toxic flame retardants like halogenated and aromatic compounds are forbidden with respect to the environmental controls [23, 24]. We report precipitation synthesis of  $\text{Al}(\text{OH})_3$  nanoparticles and polysulfone (PSu) and poly styrene (PS) nanocomposite without using any surfactants. Nanoparticles enhanced thermal stability and flame retardancy of the poly sulfone and poly styrene matrix. Nanostructures were characterized using scanning electron microscopy (SEM), transmission electron microscopy (TEM), X-ray diffraction (XRD), energy dispersive X-ray spectroscopy (EDS) and Fourier transform infrared (FT-IR) spectroscopy.

## Experimental

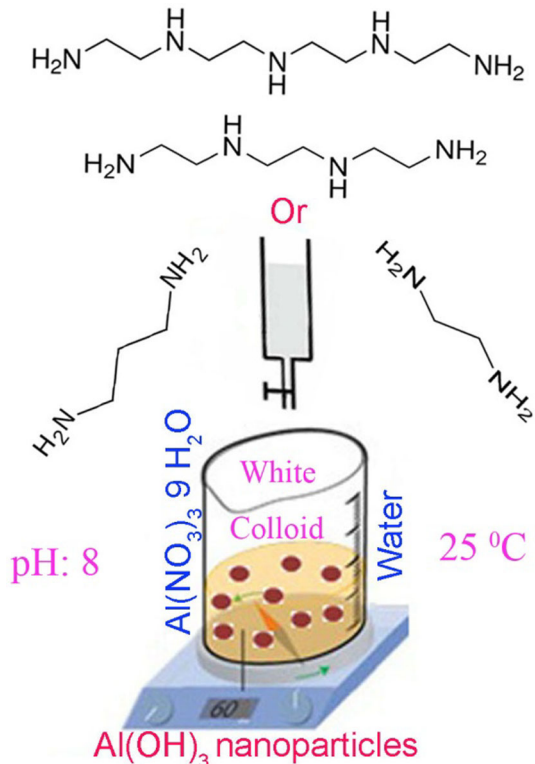
### Materials

Al(NO<sub>3</sub>)<sub>3</sub>·9H<sub>2</sub>O, ethylenediamine (ED), propylene diamine (PD), triethylenetetramine (TET), tetraethylenepentamine (TEP) were purchased from Merck Company. Poly-styrene (MW:250000) and poly-sulfone (MW:35000) were prepared from Sigma-Aldrich. All of the chemicals were used as received without further purifications.

### Synthesis of Al(OH)<sub>3</sub> and Al<sub>2</sub>O<sub>3</sub> Nanoparticles

3 g of Al(NO<sub>3</sub>)<sub>3</sub>·9H<sub>2</sub>O is dissolved in 100 mL of distilled water. Then various precipitation agents ED, PD, TET, TEP were added until the pH of the solution adjust to 8. A white precipitate is obtained confirming the synthesis of Al(OH)<sub>3</sub>. The precipitate of Al(OH)<sub>3</sub> is then centrifuged and rinsed with distilled water, followed by being left in oven to dry. Schematic of nanoparticle preparation is depicted in Scheme 1. For preparation of alumina, the products were calcinated at 750 and 900 °C for 2 h.

**Scheme 1** Schematic of preparation Al(OH)<sub>3</sub> nanoparticles

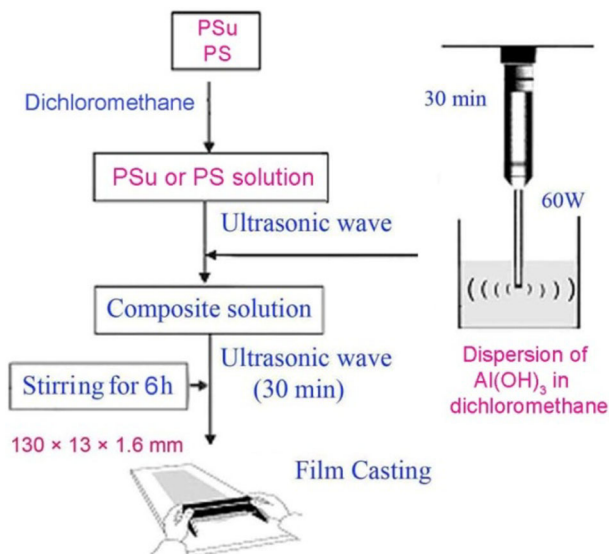


## Synthesis of Polymer–Al(OH)<sub>3</sub> Nanocomposites

For preparation of polymer–Al(OH)<sub>3</sub> nanocomposites 4.5 g of PSu (or PS) was dissolved in 10 mL of dichloromethane and then Al(OH)<sub>3</sub> (0.5 g) was dispersed in 10 mL of dichloromethane with ultrasonic waves (30 min, 60 W). The dispersion of Al(OH)<sub>3</sub> was then added slowly to the polymer solution. The solution was mixed under stirring for 6 h. For preparation of samples for UL-94 test after stirring, the product was casted on a template with dimension 130 × 13 mm and after about 24 h of solvent evaporation; the nanocomposite was placed in the vacuum oven for another 10 h for removal of residual traces of water. The final sheets for the test are 130 × 13 × 1.6 mm in dimension. Schematic of nanocomposite preparation is depicted in Scheme 2.

### Instruments

XRD patterns were recorded by a Philips, X-ray diffractometer using Ni-filtered Cu K $\alpha$  radiation. SEM images were obtained using a LEO instrument model 1455VP. Prior to taking images, the samples were coated by a very thin layer of Pt to make the sample surface conductor and prevent charge accumulation, and obtaining a better contrast. Thermo-gravimetric analysis (TGA) was carried out using an instrument (Shimadzu TGA-50H) with a heating rate of 10 °C/min under nitrogen atmosphere. A multiwave ultrasonic generator (Bandeline MS 72), equipped with a converter/transducer and titanium oscillator, operating at 20 kHz with a maximum power output of 76 W was used for the ultrasonic irradiation for dispersion of nanoparticles. TEM images were obtained on a Philips EM-208 transmission



**Scheme 2** Preparation of nanocomposite

electron microscope with an accelerating voltage of 100 kV. The influence of  $\text{Al}(\text{OH})_3$  on the fire retardancy has been considered using UL-94 test. In UL-94 a bar shape sample  $130 \times 13 \times 1.6$  mm is held vertically. A Bunsen burner flame is applied to the specimen twice (10 s each). If sample extinguished in less than 10 s after any flame application classified as V-0, drips of particles are allowed as long as they are not inflamed. A V-1 classification is given to by a sample with maximum combustion time less than 30 s, circumstances of drips are like V-0. The sample is classified V-2 if it has the combustion time criteria of V-1, but flaming drips are allowed. Samples are ranked as N.C. in UL-94 tests when the maximum total flaming time is above 50 s. The sample is classified HB when slow burning on a horizontal specimen; burning rate less than 76 mm/min [7, 23, 24].

For photo-catalytic investigation, 0.1 g of nanoparticles was dispersed in 20 ml of dye solution (3 ppm) in a quartz container. IKA magnetic stirrer with 1500 rpm was used. The UV–Vis spectra of the samples were taken on a JASCO UV–visible (Model V-670) scanning spectrometer. Halogen lamp model of GT-500, ASR, 500 W/R7s, 220–240 V/50 Hz was used for UV irradiation. Intensity and amount of  $\lambda_{\text{max}}$  of dyes were recorded firstly without presence of  $\text{Al}_2\text{O}_3$  nanoparticles. Under UV lamp irradiation and blowing of air to solution, every 10 min, sample was separated and transported to quartz cuvette in UV instrument for reading new amount of  $\lambda_{\text{max}}$  absorption.

## Results and Discussion

### Characterisation of Nanoparticles

XRD pattern of  $\text{Al}(\text{OH})_3$  nanoparticles is shown in Fig. 1. The pattern of as-prepared  $\text{Al}(\text{OH})_3$  nanoparticles is indexed as a pure monoclinic phase (space group: P21/n) which is very close to the literature values (JCPDS No. 33-0018), the narrow sharp peaks indicate that  $\text{Al}(\text{OH})_3$  nanoparticles are well crystallized.

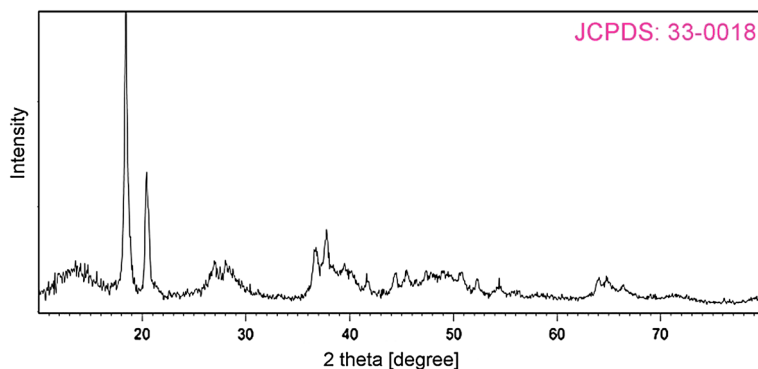


**Fig. 1** XRD pattern of the  $\text{Al}(\text{OH})_3$  nanoparticles

The crystallite size measurements were also carried out using the Scherrer equation,  $D_c = K\lambda/\beta\cos\theta$ , Where  $\beta$  is the width of the observed diffraction peak at its half maximum intensity (FWHM),  $K$  is the so-called shape factor, which usually takes a value of about 0.9, and  $\lambda$  is the X-ray wavelength (CuK $\alpha$  radiation, equals to 0.154 nm). The estimated crystallite size is about 8 nm.

Patterns of Al<sub>2</sub>O<sub>3</sub> nanoparticles prepared at 750 and 900 °C are shown in Fig. 2a, b respectively. Alumina nanoparticles show pure cubic phase (space group: Fd/3m) which have totally agreement to the literature values (JCPDS No. 29-0063). The crystallite size at 750 and 900 °C are about 5 and 4 nm respectively.

The influence of ED and PD on the morphology of the products is illustrated in Fig. 3a, b respectively. According to SEM images agglomerated nanostructures were obtained and by using ED more agglomeration was observed. Figure 3c, d show the effect of TET and TEP on the morphology of the products. By using amines that have more dentate nucleation stage overcomes growth stage and lead to nanoparticles with lower particle size.

SEM images of Al<sub>2</sub>O<sub>3</sub> nanoparticles (calcinated at 900 °C) with ED and PD are shown in Fig. 4a, b respectively and confirm formation of worm-like nanoparticles. In 900 °C in contrast to 750 °C ED and PD show lower particle size. The influence of TET and TEP on the morphology of the products is illustrated in Fig. 4c, d respectively. According to images by using TET lower nanoparticles were obtained compare to TEP.

Figure 5a shows the FT-IR spectrum of Al(OH)<sub>3</sub> nanoparticles and exhibits peaks at 520 and 1027 cm<sup>-1</sup> correspond to the Al–O bonds in Al(OH)<sub>3</sub>. Absorption peak at 3462 cm<sup>-1</sup> is because of OH groups that are adsorbed on the surface of

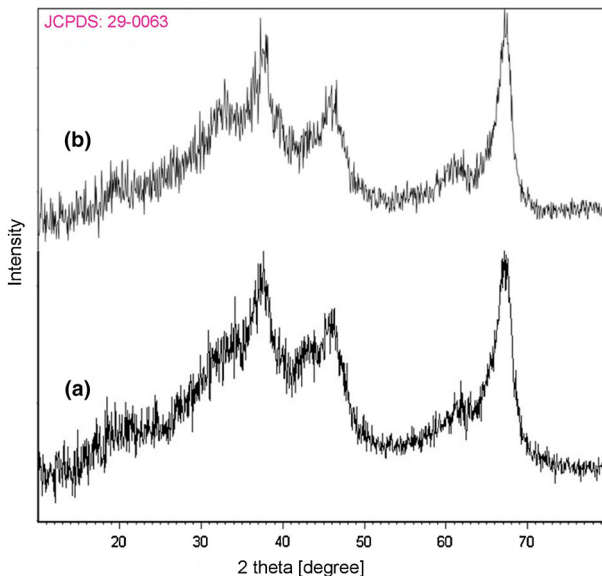


**Fig. 2** XRD pattern of the Al<sub>2</sub>O<sub>3</sub> nanoparticles at (a) 750 °C, (b) 900 °C

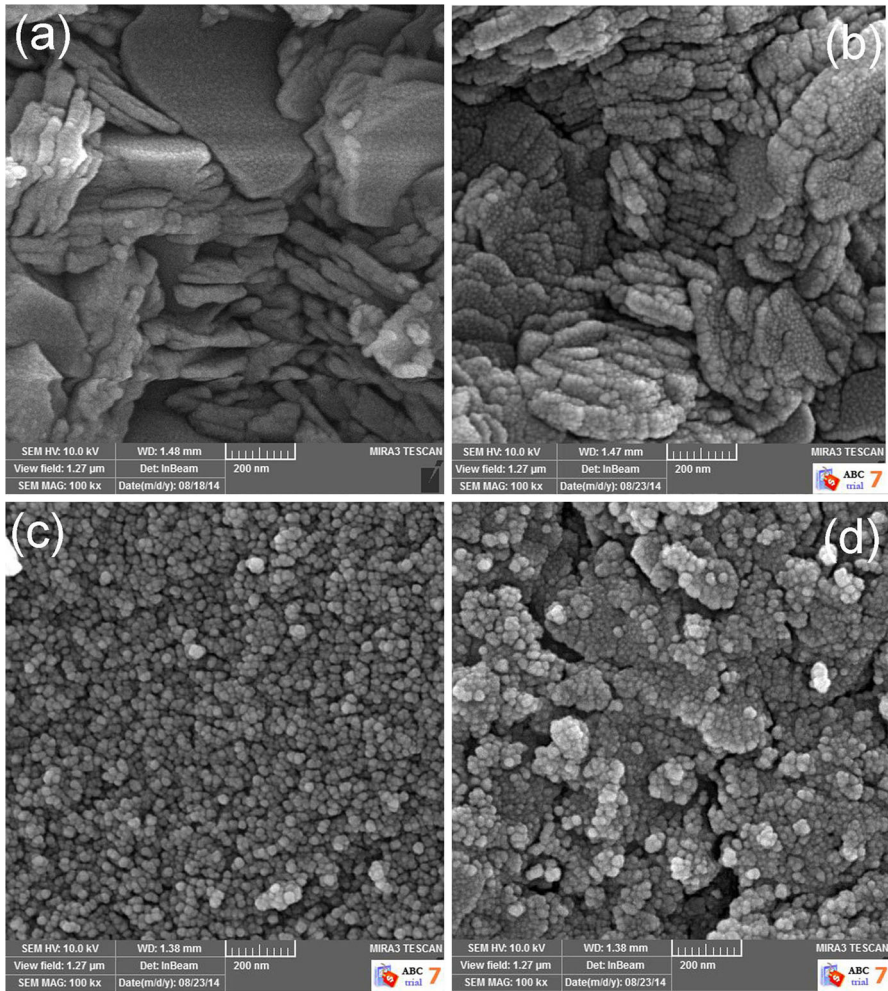


**Fig. 3** SEM images of the Al<sub>2</sub>O<sub>3</sub> at 750 °C achieved by **a** ED, **b** PD, **c** TET, **d** TEP

nanoparticles. Peak at  $3524\text{ cm}^{-1}$  is responsible to OH groups of nanoparticles. FT-IR spectrum of Al<sub>2</sub>O<sub>3</sub> is shown in Fig. 5b. As expected OH group of Al(OH)<sub>3</sub> nanoparticles is vanished. Broad peak occurs at  $3424\text{ cm}^{-1}$  is related to the O–H groups that are adsorbed on the surface of nanoparticles. Peaks at  $562$  and  $1028\text{ cm}^{-1}$  correspond to the Al–O bonds in Al(OH)<sub>3</sub>. Chemical purity of the Al(OH)<sub>3</sub> nanoparticles was analyzed by EDS. Figure 6 shows the typical EDS pattern of the sample that besides peaks of Al and O there are no other peaks for impurities.

For better estimation of particle size transmission electron microscope was used, TEM image of the product achieved by tetra ethylene pent amine is illustrated in Fig. 7 that approves product with average particle size of 20 nm.

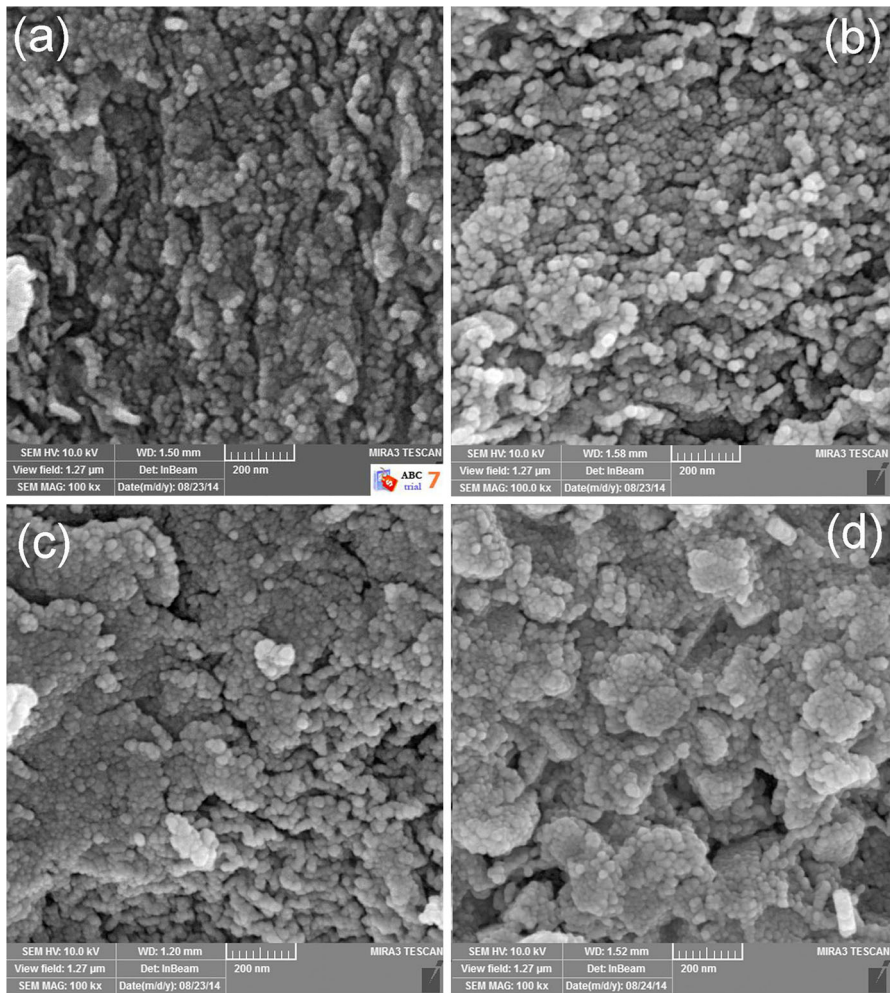
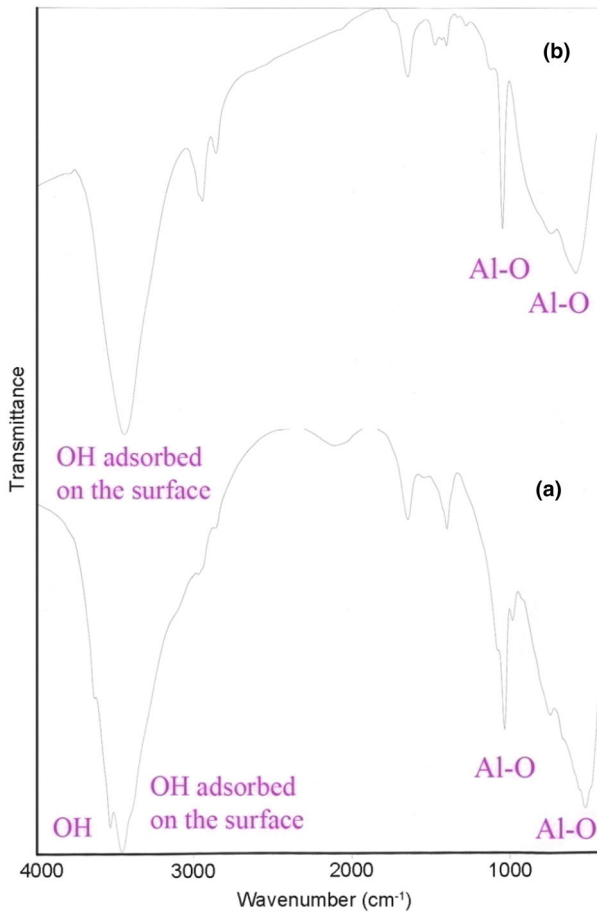


**Fig. 4** SEM images of  $\text{Al}_2\text{O}_3$  at  $900\text{ }^\circ\text{C}$  with **a** ED, **b** PD, **c** TET, **d** TEP

### Characterisation of Nanocomposites

Figure 8a shows SEM image of polysulfone– $\text{Al}(\text{OH})_3$  nanocomposite that confirms appropriate dispersion of nanoparticles in the poly sulfone matrix. SEM image of the pure polymer shows flat surface. There are some cracks in the surface, because polymer decomposes slightly under electron beam. SEM image of polystyrene– $\text{Al}(\text{OH})_3$  nanocomposite is illustrated in Fig. 8b that shows excellent regular dispersion of nanoparticles without any agglomeration in the poly styrene matrix. This dispersion can rarely be obtained by using chemical methods (SEM image of the pure polymer depicts flat and smooth surface).

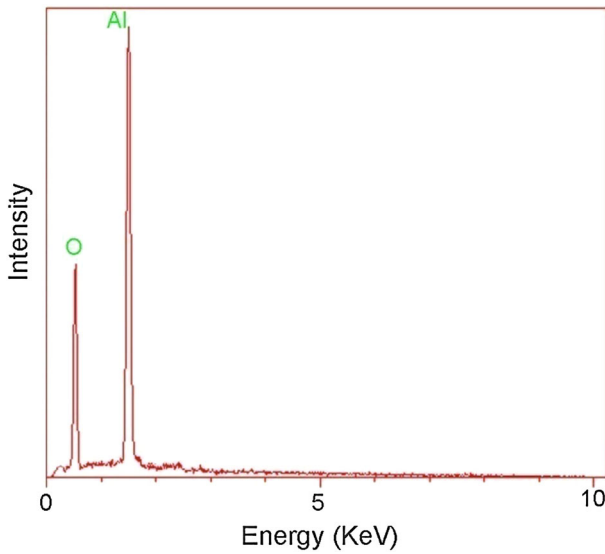




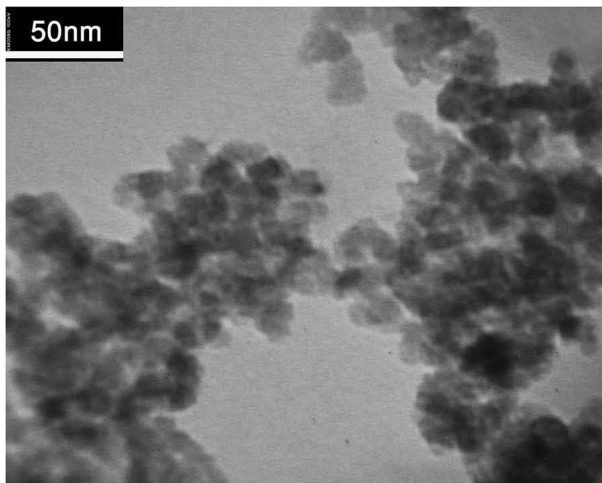
**Fig. 5** FT-IR spectra of (a)  $\text{Al}(\text{OH})_3$ , (b)  $\text{Al}_2\text{O}_3$  nanoparticles

Figure 9a shows the FT-IR spectrum of poly sulfone– $\text{Al}(\text{OH})_3$  nanoparticles and exhibits peaks at 520 and 1027  $\text{cm}^{-1}$  correspond to the Al–O bonds in  $\text{Al}(\text{OH})_3$  and confirms presence of nanoparticles in polymeric matrix. Absorption peaks at 2970 and 3064  $\text{cm}^{-1}$  are because of aliphatic and aromatic C–H bonds respectively. Peaks around 1450–1600  $\text{cm}^{-1}$  are responsible to S=O and aromatic carbon–carbon bonds and 1106  $\text{cm}^{-1}$  is responsible to C–O bond.

FT-IR spectrum of polystyrene– $\text{Al}(\text{OH})_3$  is shown in Fig. 9b. Broad peak occurs at 3300–3400  $\text{cm}^{-1}$  is related to the O–H bond. Absorption peaks at 2926 and 3060  $\text{cm}^{-1}$  are related to aliphatic and aromatic C–H bonds respectively. Peaks at 1599 and 1448  $\text{cm}^{-1}$  are correspond to aromatic carbon–carbon bonds.



**Fig. 6** EDS spectrum of  $\text{Al}_2\text{O}_3$  nanoparticles



**Fig. 7** TEM image of  $\text{Al}(\text{OH})_3$  nanoparticles

### **Photo-catalytic of $\text{Al}_2\text{O}_3$**

Methyl orange, Eriochromschwarz T and Eosin Y as typical organic pollutants were employed as targets because of the relative stability of their molecular structure. The alumina nanoparticles have the potential to be applied to improve environmental problems associated with organic and toxic water pollutants. The photo-catalytic activity of the nanoparticles was evaluated by monitoring the degradation of dyes in

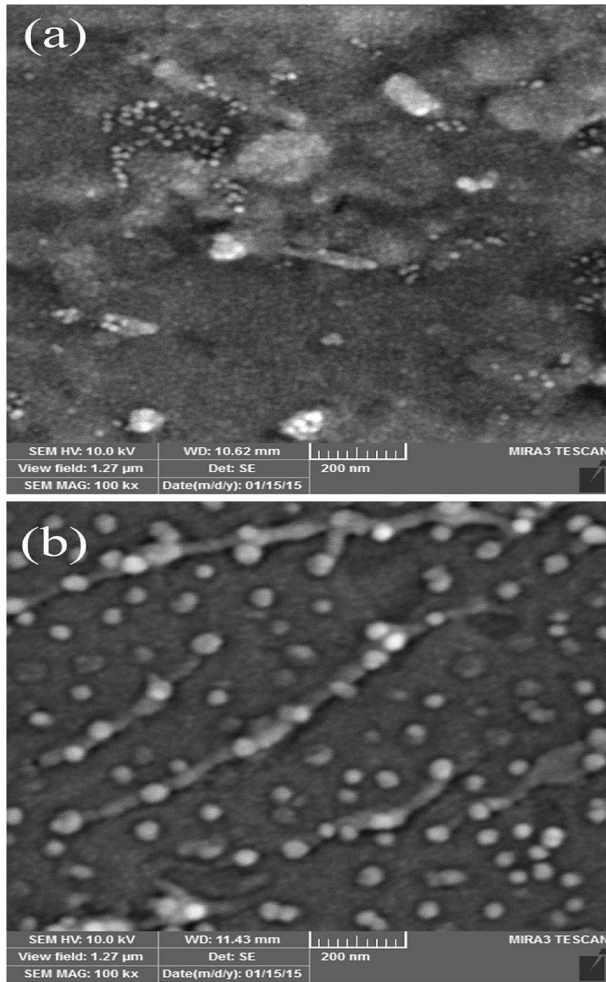


**Fig. 8** SEM images of **a** PSu- $\text{Al}(\text{OH})_3$ , **b** PS- $\text{Al}(\text{OH})_3$  nanocomposite

an aqueous solution, under irradiation with UV light. The changes in the amount of  $\lambda_{\text{max}}$  (degradation percent) are illustrated in Fig. 10. As time increased, more and more dye are adsorbed on the nanoparticles catalyst, until the absorption peaks ( $\lambda_{\text{max}}$ ) of Methyl orange, Eriochromschwarz T, Eosin Y (that are 510, 516 and 615 nm respectively) decrease and vanish around 100 min. More than 90 % of Eosin Y was degraded at 100 min of irradiation. 60–70 % of two others were degraded at 80 min of irradiation. The dyes concentration decreased rapidly with increasing UV-irradiation time, and the absorption peaks almost disappeared after 100 min. Organic dyes decompose to carbon dioxide, water and less toxic or nontoxic residuals.

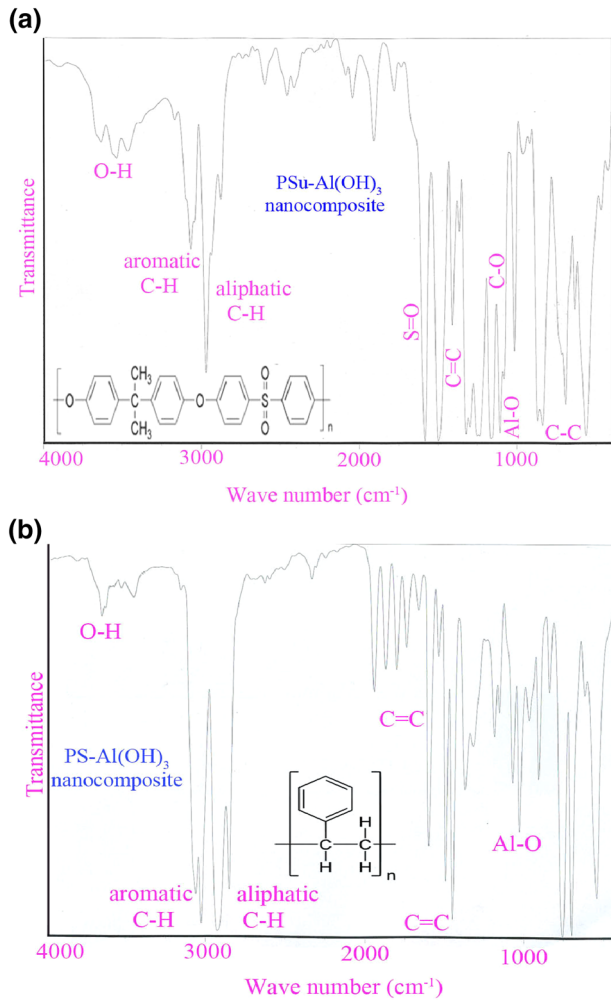


**Fig. 9** FT-IR spectra of **a** PSu-Al(OH)<sub>3</sub>, **b** PS-Al(OH)<sub>3</sub> nanocomposite

### Thermal Stability and Flame Retardancy

Thermal stability of the pure polymer and nanocomposite was investigated by TGA. TGA curves of PS and PS-Al(OH)<sub>3</sub> nanocomposite are shown in Fig. 11a, b respectively. Because of present of Al(OH)<sub>3</sub>, thermal decomposition of the nanocomposite was shifted towards the higher temperatures. Dispersed Al(OH)<sub>3</sub> nanoparticles can act as barriers which slow down product volatilization and thermal transport during decomposition of the polymer.

The results show that the Al(OH)<sub>3</sub> can enhance the flame retardant property of the polymeric matrix. The outcomes of UL-94 tests for pure PS is N.C while PS-Al(OH)<sub>3</sub> and PSu-Al(OH)<sub>3</sub> show V-0 state. The higher level of flame retardancy of

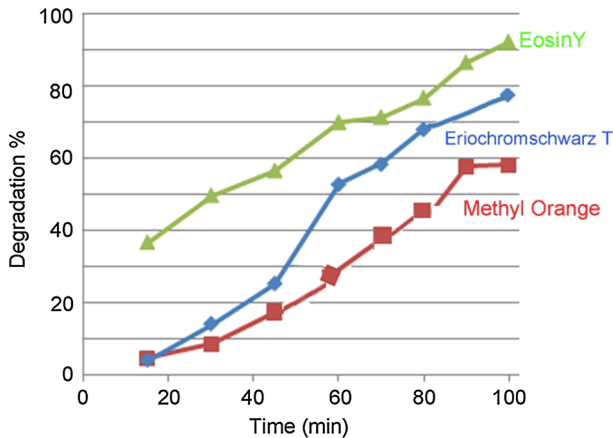


**Fig. 10** Degradation versus time at presence of  $\text{Al}_2\text{O}_3$  nanoparticles

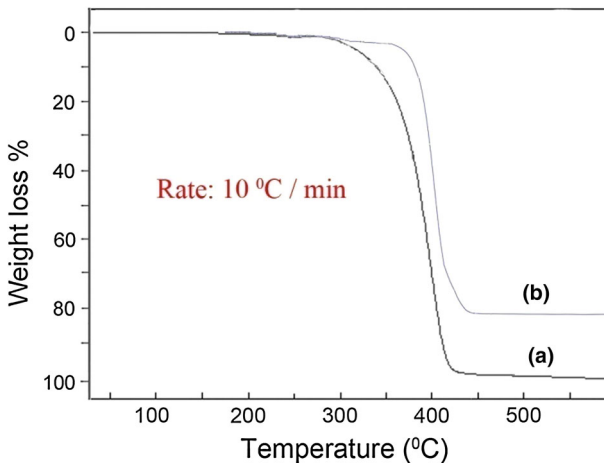


**Fig. 11** TGA of (a) pure PS (b) PS- $\text{Al}(\text{OH})_3$  nanocomposite

nanoparticles is due to their bigger surface to volume fractions which let them to disperse into the polymeric matrix homogeneously, and hence leads to formation of a compact char during the combustion. The enhancement of flame retardancy of nanocomposite is due to endothermic decomposition of  $\text{Al}(\text{OH})_3$  that absorbs energy and simultaneously releases of water (dilutes combustible gases). Hydroxyl groups on the surface of  $\text{Al}(\text{OH})_3$  have suitable interaction with sulfonyl of PSu. After decomposition of aluminum hydroxide,  $\text{Al}_2\text{O}_3$  and char remain as a barrier layer. This obstruction slows down evaporation of polymeric segments and prevents reaching oxygen, heat and flame to the product [7, 23, 24].

Bulk micro structure  $\text{Al}(\text{OH})_3$  was added to polymers. There was unsuitable dispersion of bulk  $\text{Al}(\text{OH})_3$  in polymer matrices therefore separated inorganic and polymer phases were obviously observed even by unaided eye. There were cracks in

boundary of bulk additives and polymeric matrix which reduce mechanical stability of composite. For pass flame retardancy tests, 30–65 wt% of bulk aluminum hydroxide is required while in this work by applying 10 % of nanostructure flame retardancy and thermal stability enhanced.

## Conclusions

Al(OH)<sub>3</sub> nanoparticles were synthesized via a simple surfactant-free precipitation reaction at room temperature. Nanoparticles were characterized using XRD, SEM, TEM, EDS and FT-IR techniques. The effect of different parameters such as precipitating agents and temperature on the morphology of the products was investigated. Al(OH)<sub>3</sub> show suitable dispersion into poly styrene. The results show that the nontoxic nano-fillers can appropriately improve thermal stability and flame retardancy of the polymeric matrices because of endothermic decomposition that release water simultaneously. It was found that the as-obtained Al<sub>2</sub>O<sub>3</sub> nanoparticles exhibit photo-catalyst property under UV light.

**Acknowledgments** Authors are grateful to council of University of Kashan for providing financial support to undertake this work by Grant No (159271/295).

## References

1. F. Laoutid, L. Bonnaud, M. Alexandre, J. Lopez-Cuesta, and Ph. Dubois (2009). *Mater. Sci. Eng. R* **63**, 100.
2. D. Ghanbari, M. Salavati-Niasari, and M. Sabet (2013). *Compos. B* **45**, 550.
3. A. B. Morgan and C. A. Wilkie *Flame Retardant Polymer Nanocomposite, Chapter 1* (Wiley, New Jersey, 2007).
4. B. Y. Geng, J. Z. Ma, and J. H. You (2008). *Cryst. Growth Des.* **8**, 1443.
5. D. Ghanbari, M. Salavati-Niasari, and M. Sabet (2012). *J. Clust. Sci.* **23**, 1081.
6. B. Jia and L. Gao (2008). *J. Phys. Chem. C* **112**, 666.
7. D. Ghanbari, M. Salavati-Niasari, and M. Ghasemi-Kooch (2014). *J. Ind. Eng. Chem.* **20**, 3970.
8. X. Sun, C. Zheng, F. Zhang, Y. Yang, G. Wu, A. Yu, and N. Guan (2009). *J. Phys. Chem. C* **113**, 16002.
9. S. Liu, J. Ying, X. Zhou, and X. Xie (2009). *Mater. Lett.* **63**, 911.
10. F. Gholamian, M. Salavati-Niasari, D. Ghanbari, and M. Sabet (2013). *J. Clust. Sci.* **24**, 73.
11. H. Wang, P. Fang, Z. Chen, and S. Wang (2007). *Appl. Surf. Sci.* **253**, 8495.
12. P. Jamshidi, M. Salavati-Niasari, D. Ghanbari, and H. R. Shams (2013). *J. Clust. Sci.* **24**, 1151.
13. F. Gholamian, G. Nabyouni, D. Ghanbari, R. Jalajerdi, and A. Aminifazl (2013). *High Temp. Mater. Proc.* **32**, 125.
14. W. Q. Cai, J. G. Yu, and M. Jaroniec (2010). *J. Mater. Chem.* **20**, 4587.
15. N. K. Renuka, A. V. Shijina, and A. K. Praveen (2012). *Mater. Lett.* **82**, 42.
16. Y. K. Park, E. H. Tadd, M. Zubris, and R. Tannenbaum (2005). *Mater. Res. Bull.* **40**, 1506.
17. F. Yaripour, Z. Shariatinia, S. Shariatinia, and A. Irandoukht (2015). *Fuel* **139**, 40.
18. A. A. Pechenkin, S. D. Badmaev, and V. D. Belyaev (2015). *Appl. Catal. B* **166**, 535.
19. T. K. Ghosh and N. N. Nair (2015). *Surf. Sci.* **632**, 20.
20. S. Y. Hosseini and M. R. K. Nikou (2014). *J. Ind. Eng. Chem.* **20**, 4421.
21. P. Manivasakan, A. Karthik, and V. Rajendran (2013). *Powder Technol.* **234**, 84.
22. X. Wu, B. Zhang, and Z. Hu (2013). *Powder Technol.* **239**, 155.
23. P. Jamshidi, D. Ghanbari, and M. Salavati-Niasari (2014). *J. Ind. Eng. Chem.* **20**, 350.
24. M. Yousefi, E. Noori, D. Ghanbari, M. Salavati-Niasari, and T. Gholami (2014). *J. Clust. Sci.* **25**, 397.